Catalysis Today 161 (2011) 169–174

Contents lists available at ScienceDirect

Catalysis Today

journal homepage: www.elsevier.com/locate/cattod

Photocatalytic removal of ethanol and acetaldehyde by N-promoted TiO_2 films: The role of the different nitrogen sources

D. Meroni [a,*], S. Ardizzone [a], G. Cappelletti [a], C. Oliva [a], M. Ceotto [a], D. Poelman [b], H. Poelman [b]

[a] Dipartimento di Chimica Fisica ed Elettrochimica, Università di Milano, Via Golgi 19, 20133 Milano, Italy
[b] Department of Solid State Sciences, Ghent University, Krijgslaan 281, B-9000 Gent, Belgium

ARTICLE INFO

Keywords:
N-doped TiO_2
Photocatalytic degradation
Ethanol
Acetaldehyde

ABSTRACT

Pure and N-doped TiO_2 nanoparticles are obtained by a combination of wet and thermal procedures, starting from $TiCl_3$ and alkoxide precursors; the N-source is both inorganic (NH_3) and organic (triethylamine). Samples are characterized for their bulk, surface, optical and magnetic properties. Ab initio calculations of the electronic properties of the doped samples are performed. Sample thin films are tested for their photocatalytic activity, under UV and simulated solar irradiation, with respect to air pollutants ethanol and acetaldehyde. Both the disappearance of the molecule itself and the complete mineralization (CO_2) are followed during the reaction time. FTIR/ATR analyses are performed on samples withdrawn during the course of the reaction to identify reaction intermediates. In the case of acetaldehyde, photocatalytic tests are also performed under visible light ($\lambda > 400$ nm). The photoactivity sequences of the N-doped samples under the different irradiation sources are discussed with reference to their surface/bulk properties, light absorption features, nature and amount of paramagnetic species.

1. Introduction

Ethanol is an important atmospheric pollutant: it is a commonly used industrial solvent and a fuel additive; it is also produced by breweries and bakeries. Its emissions accounted for about 4% of anthropogenic emissions of VOCs in the UK in 1993 [1]. Atmospheric concentrations of this pollutant are expected to rise in consequence of the use of ethanol as biofuel in the automotive sector. Several studies performed in large Brazilian cities, where a substantial part of vehicles are fueled by ethanol, showed very high atmospheric concentrations of this pollutant [2]. Moreover, it is well established that the use of ethanol as fuel leads to an increase in the atmospheric levels of acetaldehyde, which is far more toxic and reactive in the atmosphere than the original ethanol [3,4]. Besides, acetaldehyde is an important indoor pollutant itself, released by some building materials such as polyurethane foams, and some consumer products such as cigarettes, adhesives, coatings and inks. Generally, acetaldehyde concentrations are higher indoors than outdoors. Ethanol and acetaldehyde emissions are reduced but not eliminated by catalytic converters [5].

Photocatalytic oxidation of pollutants is one of the most promising technologies in environmental protection and remediation, especially for the removal of low concentration pollutants in slightly contaminated enclosed atmospheres. TiO_2 is the most frequently employed photocatalyst owing to its cheapness, non-toxicity, structural stability and higher activity.

Photocatalytic degradation of ethanol over TiO_2 both in gas and in liquid phase has been extensively investigated by several authors [6–14]. Nonetheless, there is still no general agreement on the reaction mechanism and the related kinetic description. Acetaldehyde has widely been acknowledged as the main gaseous intermediate. Several authors found lower concentrations of other byproducts, such as acetic acid and formaldehyde. CO_2 and water are invariably the final products of the oxidation over TiO_2.

One of the most appealing aspects of photocatalysis is the possibility of exploiting solar light and even common artificial light sources to activate the catalytic process. In this regard, a main disadvantage of TiO_2 compared with other semiconductors is its large band gap ($\geq$3 eV), which corresponds to an absorption edge in the UV. As only 5% of solar radiation is in the UV region, a shift towards visible absorption is required in order to improve the photocatalytic activity of TiO_2 under solar irradiation. Doping with non-metals, such as nitrogen, is currently considered a very promising approach to TiO_2 visible-sensitization. Absorption spectra of N-doped samples invariably exhibit a shift to the visible region, regardless of the preparative method employed and of the nitrogen source. Although these materials absorb visible light, they are nonetheless frequently inactive in photooxidation, probably because of charge recombination effects [15]. Thus, visible-light photoactivity of N-doped TiO_2 appears to be highly sensitive to the preparative routes.

* Corresponding author. Tel.: +39 0250314219; fax: +39 0250314228.
E-mail address: daniela.meroni@unimi.it (D. Meroni).

0920-5861/$ – see front matter © 2010 Elsevier B.V. All rights reserved.
doi:10.1016/j.cattod.2010.08.013

Here, N-doped TiO_2 films are obtained by different synthetic routes (sol–gel and precipitation method) and different N-sources (organic and inorganic). Both particles and films are characterized by structural, morphological and surface features. The photocatalytic activity of the films is tested for the oxidation of both ethanol and acetaldehyde. The sequence of the photoactivity of the N-doped samples under different irradiation sources is discussed in relation to their surface/bulk properties, light absorption features, nature and amount of paramagnetic species.

2. Experimental

2.1. TiO_2 preparation

All chemicals were of reagent grade purity and were used without further purification.

N-doped TiO_2 samples were prepared using two different synthetic techniques: a sol–gel method from an alkoxide precursor and a precipitation method from a $TiCl_3$ precursor. In the case of sol–gel samples, two sources of N-dopant were adopted: inorganic (NH_3) or organic (triethylamine, tea).

The preparation of TiO_2 samples by the sol–gel technique was performed following a procedure previously reported [16]: a solution of 0.063 mol of $Ti(OC_3H_7)_4$ in 24 mL of 2-propanol was stirred for 10 min at 300 rpm. An aqueous solution containing the base necessary to obtain a final pH of 9 was prepared separately: KOH was adopted in the case of the undoped TiO_2 sample (**Tsg**) and of the tea-doped sample (**Tsg_tea**). In the latter, the N-source (tea, N/Ti initial molar ratio = 0.1) was also added to the base solution. Instead, the base adopted in the case of the NH_3-doped sample (**Tsg_NH$_3$**) was a buffer solution containing NH_3 and $(NH_4)_2CO_3$ (N/Ti initial molar ratio = 0.7). 114 mL of the alkaline aqueous solution were added, dropwise, fast, to the alkoxide solution, in order to obtain a water/alkoxide molar ratio of 100 and a water/2-propanol molar ratio of 20. The slurry was stirred for 90 min at 25 °C in order to complete the hydrolysis. The obtained precursor was dried to a xerogel. Dry powders were washed with milli-Q water by centrifugation and suspension cycles, till the washing solution conductivity was <1 mS. Finally the powders were calcined at 400 °C for 6 h under O_2 stream (9 NL/h).

The sample from $TiCl_3$ (**Tp_NH$_3$**) was prepared using the procedure described in [17]. A final pH value of 9 was adopted and the resultant N/Ti initial molar ratio was of 7.0. The sample was extensively washed at the end of the synthetic process.

The actual N/Ti ratios of the N-doped samples, determined by XPS analysis, range around 0.015–0.022. These values are much lower (one or two order of magnitudes) than the starting molar ratios adopted in the different synthetic routes. Apparently an appreciable loss of N containing species occurs during calcination, as previously reported [16,17]. As all samples contain the same nitrogen amount at the surface, they can be compared.

2.2. Sample characterization

Room-temperature X-ray powder diffraction patterns were collected between 10 and 80 °C with a Siemens D5000 diffractometer, using Cu Kα radiation. Rietveld refinement has been performed as in Ref. [16]. The average diameter of the crystallites was estimated by the Scherrer equation [18].

Specific surface areas were determined by the BET procedure using a Coulter SA 3100 apparatus.

Diffuse reflectance measurements in the UV/vis region were performed using a procedure previously described [16,19].

Scanning electron microscopy (SEM, FEI Quanta 200F FEG) in high vacuum mode was used to characterized the particle morphology.

Electron paramagnetic resonance (EPR) spectra were collected at room temperature using a Bruker Elexsys X-band spectrometer at the working frequency of about 9.4 GHz. The spectral simulations were obtained by the Bruker SimFonia program [20].

The particle populations of all samples were analyzed by a Beckman Coulter N4 analyzer.

To model the effect of N-doping, periodic three-dimensional DFT calculations were carried out using the VASP 4.6 code [21] with the projector augmented wave (PAW) method [22]. The generalized gradient approximation (GGA) by Perdew et al. [23] was employed and the plane wave basis set cutoff was 400 eV. Geometry optimization with the conjugated gradient scheme was stopped when the forces on the atoms were less than 0.05 eV/Å. The DOS (Density of electronic States) for a $3 \times 3 \times 3$ supercell model was calculated both at the Γ point of the Brillouin zone and using a $2 \times 2 \times 2$ Monkhorst-Pack set of *k*-points to check basis set convergence.

2.3. Photocatalytic experiments

Gas-phase photocatalytic tests were performed with respect to two different pollutants (ethanol and acetaldehyde). Two experimental set-ups and film deposition procedures were utilized; these dispositions were previously developed and adopted for the two pollutant molecules themselves [24,25].

The study of the photocatalytic oxidation of ethanol was performed at 313 K in a custom-made batch reactor equipped with a UV lamp, that has been described previously [24,26]. The TiO_2 thin films (area 9.3 cm^2) were deposited by spin coating on sodium-free glass. The initial reaction rate was determined from the slope of the first linear data points of ethanol breakdown. Ethanol adsorption onto the TiO_2 layer was determined through dark experiments: no appreciable amount was detected.

Photocatalytic degradations of acetaldehyde were conducted at 308 K in a Pyrex glass cylindrical reactor with diameter of 200 mm and effective volume of 5 L [17]. The reaction chamber was filled with a N_2/O_2 dry atmosphere (ratio 80:20). Thin TiO_2 films were deposited by drop casting using isopropanol as a solvent onto a glass plate (area 66.4 cm^2). Acetaldehyde was injected using a microsyringe into the reaction chamber up to an initial concentration of 300 ppm. The actual concentration of acetaldehyde in the reactor was determined directly by micro-GC sampling (3000A Agilent Technologies, equipped with RT PLOT Q and OV-1 columns and TCD detectors). After the pollutant injection, the system was held in the dark for an equilibration time of 15 min in order to evaluate the adsorption of the pollutant at the catalyst surface. The amount of adsorbed acetaldehyde ranged from 25 to 50 ppm, depending on the sample adsorption properties. Photon sources were provided by an UV 500 W iron halogenide lamp (Jelosil HG 500, photon flux 2.4×10^{-5} E dm^{-3} s^{-1}, emission spectra see Fig. S1a in Supporting information) and by a 300 W solar lamp (Radium Sanolux HRC 300-280, photon flux 1.2×10^{-5} E dm^{-3} s^{-1}, emission spectra see Fig. S1b). The concentrations of acetaldehyde and of the product of complete mineralization were followed during the entire reaction time using the micro-GC. The chemical structure of the organic compounds remaining on the TiO_2 surface was analyzed using Fourier transform infrared spectroscopy (FTIR; Jasco 4200, accessorized by attenuated total reflectance (ATR) module). The spectra of the species adsorbed at the catalyst surface were obtained by subtracting the curves of the as prepared samples from the spectra of the used catalyst. Acetaldehyde adsorption onto the TiO_2 layer was determined through dark experiments: the adsorption phenomena account for the disappearance of 5–10% of acetaldehyde after 3 h, depending on the sample adsorption features.

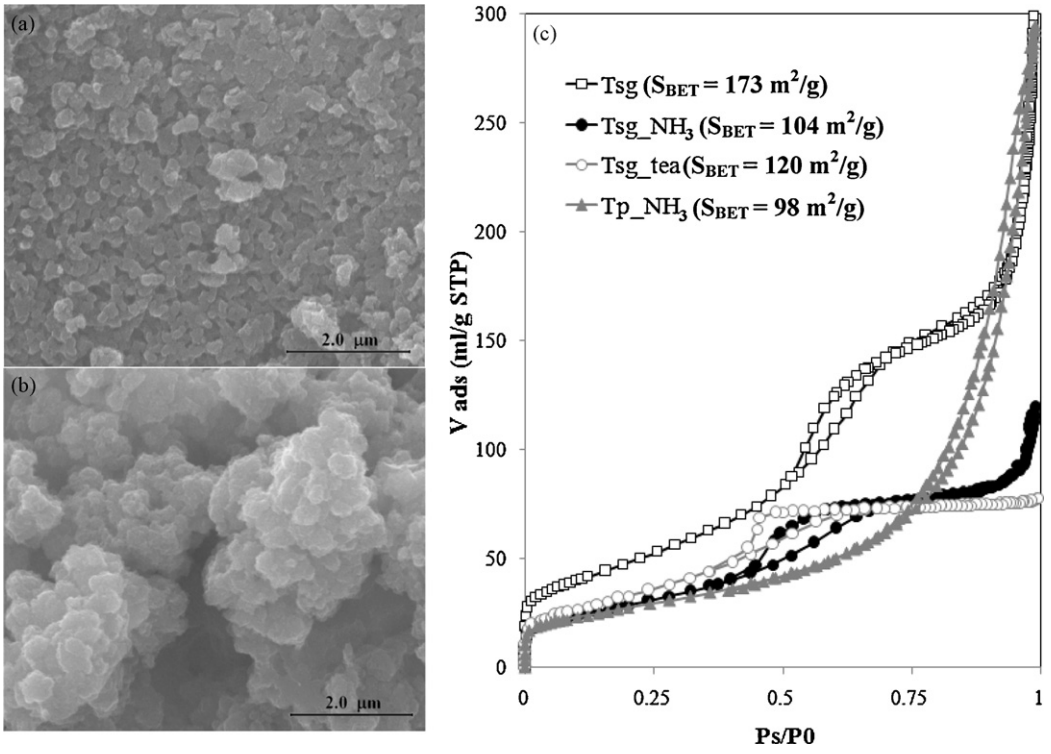

Fig. 1. Sample morphology: SEM images of (a) Tsg and (b) Tsg_NH_3; (c) N_2 adsorption isotherms with relative hysteresis loops and BET surface area of all samples.

Photolysis experiments (in the absence of photocatalyst) were performed for both molecules: no appreciable degradation was observed.

3. Results and discussion

3.1. Structural and morphological characterization

The sample phase composition is remarkably influenced by the addition of nitrogen. In agreement with previous results [16], N-doping seems to promote the anatase phase, even if the different N-sources have a diverse impact. As shown by sample X-ray diffraction lines (Fig. S2), the undoped TiO_2 shows the distinctive peaks of both anatase ($2\theta_{101} = 25.31^\circ$) and brookite ($2\theta_{211} = 30.81^\circ$). The tea-doped sample presents only a slight decrease in the brookite content. Changing the N-source markedly influences the phase composition and crystallite size: the NH_3-doped samples consist of almost pure anatase, with no appreciable peaks related to brookite. The increase in anatase polymorph is accompanied by an expected increase in the crystallite size (9, 15, 17 nm for Tsg_tea, Tsg_NH_3 and Tp_NH_3, respectively) with respect to the undoped Tsg value (7 nm).

Nitrogen addition affects the sample morphology as well. The surface area of N-doped samples decreases as a consequence of the crystallite growth and sintering (Fig. 1c). The aggregation phenomena linked to N-doping are appreciable in SEM images shown in Fig. 1a and b, which compare the undoped Tsg with the more aggregated Tsg_NH_3. SEM pictures are in agreement with granulometric measurements: Tsg presents an average particle dimension of ca. 300 nm, whereas Tsg_NH_3 has a grain size of around 700 nm.

The adopted synthetic route plays also a relevant role in affecting the sample porosity. As apparent from Fig. 1c, the shape and volume distribution of sample pores are influenced by the adopted synthetic pathway. In particular, the sol–gel synthesis leads to bottleneck pores and to greater percentages of smaller pores ($d < 6$ nm), whereas the precipitation method results in slit-shaped pores of larger dimensions.

3.2. Optical, electronic and magnetic properties

In Fig. 2 the diffuse reflectance (DR) UV–vis spectra of the bare TiO_2 (curve 1) and the N-doped samples (curves 2–4) are compared. The corresponding derivative plot is shown in Fig. S3. The increased absorption in the visible region can be related to the presence of nitrogen (either interstitial or substitutional) in the oxide, in analogy with what was previously reported for N-doped TiO_2 nanoparticles [16,27,28]. The "apparent" band gap values, according to the Kubelka–Munk equation [16], are reported in Fig. 2a (inset table). For all N-doped samples a band gap narrowing is observed; this effect can be attributed to electronic transitions from intragap localized levels to the conduction band, as reported by several authors [15]. The largest shift is found for the sample Tsg_tea (2.98 eV).

Electronic structure properties for the N-doped TiO_2 described above obtained by DFT calculations are reported in Fig. 2b. The presence of both substitutional and interstitial N species generates intragap localized states, which might support the apparent band gap narrowing reported in Fig. 2a.

EPR measurements were performed on the N-doped samples, in order to analyze the paramagnetic species induced by the N-doping itself. EPR spectra of N-doped samples were recorded 24 h after the calcination.

Tsg_NH_3 and Tsg_tea give rise to EPR spectra with similar patterns but very different spectral intensities (Fig. 3a and b). In particular, the spectral intensity of Tsg_NH_3 is 1.46 times higher than that of Tsg_tea. The spectral profiles of both samples are simulated by hypothesizing an unpaired electron with Zeeman energy parameters $g_x = 2.0066$; $g_y = 2.0054$; $g_z = 2.0040$ and interacting with a nuclear magnetic moment $I = 1$ through the hyperfine coupling parameters $A_x \approx A_y \approx 3$G and $A_z \approx 32.2$G. This pattern can

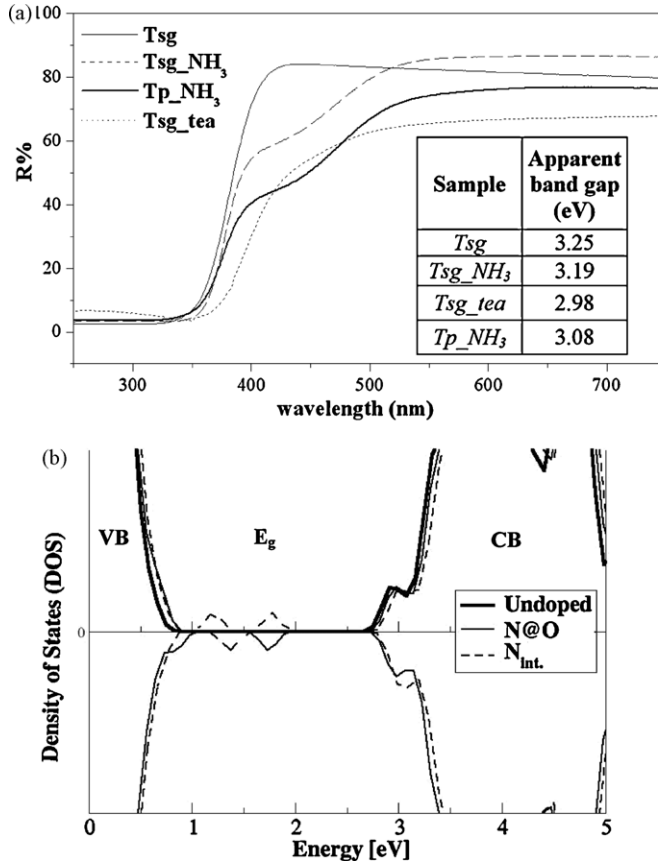

Fig. 2. (a) DRS spectra of all samples. Their apparent band gap values are reported in the inset table. (b) Calculated spin polarized density of electronic states (DOS) for undoped, substitutional and interstitial N-doping at a N/Ti stoichiometric ratio of 0.0185. Upper and lower panels for different spins.

be attributed to $N_b^{\bullet}$, i.e. to a nitrogen paramagnetic defect located in the bulk of the N-TiO_2 nanocrystals [16].

A completely different EPR pattern is obtained for Tp_NH_3 (Fig. 3c). Its intense and broad feature is similar to that previously reported by our group in [17] for the same preparation route. Some attributions were tentatively proposed there for such a low-resolution pattern. A trace of the $N_b^{\bullet}$ EPR signal is also found in this pattern, by subtracting from it the EPR spectrum of a sample

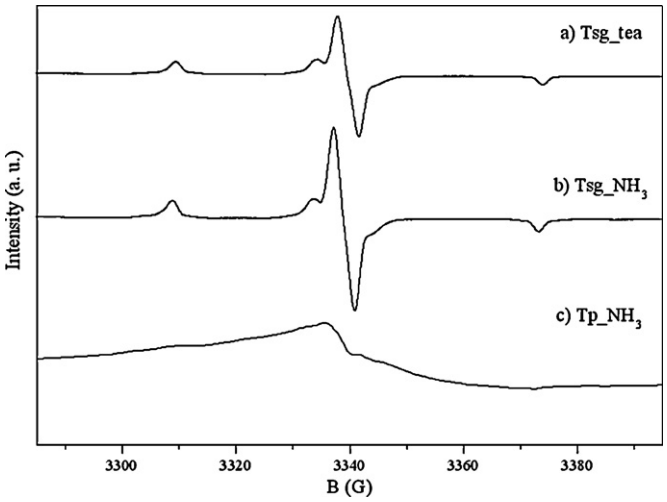

Fig. 3. EPR spectra of N-doped samples: (a) Tsg_tea, (b) Tsg_NH_3, (c) Tp_NH_3.

prepared following an identical synthetic pathway but with lower dopant amount.

3.3. Photocatalytic experiments under UV

All samples were tested for the photocatalytic removal of ethanol and, separately, of its main degradation intermediate, acetaldehyde. Photocatalytic tests were performed using different irradiation sources, in order to understand how the diverse sample characteristics influence the photocatalytic activity under different conditions. The photocatalytic activities of every sample were compared with respect to:

a. the removal of two different pollutants under the same kind of light irradiation (UV);
b. the oxidation of the same pollutant (acetaldehyde) under UV, simulated solar and visible irradiation.

Fig. 4 compares two representative curves of ethanol and acetaldehyde photocatalytic degradation under UV irradiation in the two experimental set-ups.

Regarding ethanol photocatalytic oxidation, the concentration of ethanol was quantitatively monitored in time using the MS peak at 45 amu, while the CO_2 concentration was followed only qualitatively. Fig. 4a shows that the ethanol concentration decreases sharply at the beginning of the reaction, then it starts to increase reaching a quasi-plateau region. The apparent minimum in the ethanol concentration is due to a CO_2 isotope that gives its peak at 45 amu. In fact, the increase of the mass/charge signal at 45 amu coincides with a strong increase in the mass/charge signal at 44 amu, which is the signal of CO_2. As a result, it is not significant to follow the ethanol signal further than its minimum, since it is then biased by the increasing CO_2 concentration. Therefore, the photocatalytic activities of the different catalysts are compared using the method of initial decay [26]. Initial rates of ethanol photodegradation (r_{init}^{EtOH}) were obtained from the tangent of the initial part of the ethanol curve – the slope of the straight line interpolating the first 100 points. The same procedure was adopted in the case of acetaldehyde photocatalytic tests (r_{init}^{Ac}).

In agreement with previous literature results, a Langmuir–Hinshelwood kinetic model can be proposed for the present degradation of ethanol, while the acetaldehyde breakdown follows a pseudo-zero order kinetics. The difference in the observed reaction order between acetaldehyde and ethanol can be attributed to the competition in adsorption between ethanol and its main degradation intermediate, acetaldehyde.

In acetaldehyde degradation experiments, the concentrations of both acetaldehyde and CO_2 were quantitatively followed by gas-chromatography. No other GC peaks were detected during the tests. The final CO_2 concentrations (600 ppm) indicate the occurrence of a complete mineralization after less than 150 min for all samples. A complete mineralization of ethanol was also always achieved in less than 140 min (except in the case of Tsg_tea), since a plateau region in the CO_2 curve was always obtained. The end of the reaction was assessed also by ATR-IR analysis of the film surface, which showed only peaks that could be attributed to H_2O_{ad} (δ(OH) at 1635 cm^{-1}) and to CO_3^{2-} (ν_s(COO) at 1400 cm^{-1}) [10]. The absence of reactant molecules or byproducts at the end of the reaction shows that no catalyst poisoning occurs. Surface area tests of used catalysts indicate that no morphological modifications take place during the reaction.

Table 1 (2nd and 4th columns) shows the initial rates determined for all samples in the different photocatalytic tests. Tsg_NH_3 is the most active sample in both tests under UV irradiation. Its initial rates of photodegradation are slightly higher than those of Tsg. The improved activity of Tsg_NH_3 is even more striking if spe-

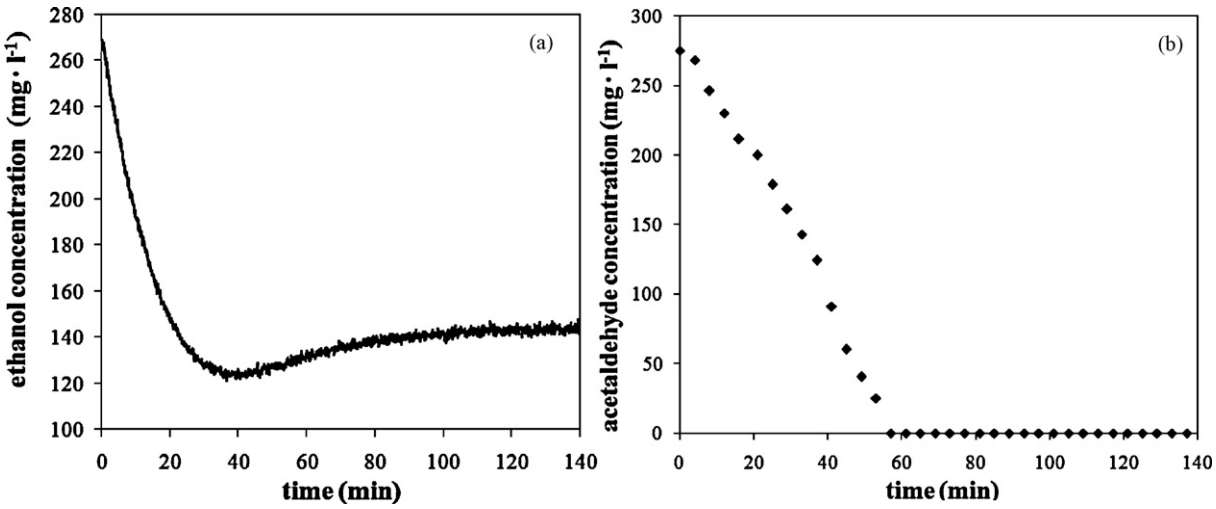

Fig. 4. Representative pollutant degradation curves for the photocatalytic oxidation of (a) ethanol and (b) acetaldehyde under UV irradiation.

cific degradation percentages are considered, i.e. with respect to the actual surface area of each sample (Table 1 3rd and 5th columns). The other N-doped samples exhibit a much lower activity. Specifically, Tsg_tea is the less active, the more so for ethanol degradation.

The same sequence of catalytic activity was devised with respect to the two pollutants. This fact suggests that acetaldehyde is the main intermediate in ethanol photocatalytic oxidation, in agreement with the larger part of literature [6–14], and that its degradation is the rate determining step of the reaction. However, it should be stressed that results reported in Table 1 refer to different experimental set-ups and different light sources, therefore they cannot be directly compared, as the light source intensity was different in these cases. Nonetheless, the photocatalytic sequence of activity can still be compared.

During our tests of acetaldehyde breakdown, no intermediate species were detected using gas-chromatography. An attempt to identify reaction intermediates not detectable by GC, was carried out using FTIR. FTIR analyses were performed on the surface of TiO_2 catalysts withdrawn from the reaction chamber after half of the time necessary for a complete acetaldehyde removal.

According to the peak attribution proposed by Yu and Chuang [14], several species can be identified (Fig. 5). Adsorbed acetaldehyde gives rise to the presence of a peak at 1716 cm^{-1}. The products of complete mineralization give also characteristic bands ($CO_{2,ad}$ at 2363 cm^{-1} and H_2O_{ad} at 1651 cm^{-1}). The distribution of the superficial OH groups seems to change with respect to the as prepared catalyst. Specifically, the peak component at 3730 cm^{-1} increases while the broad band centered around 3300 cm^{-1} markedly decreases in intensity. Other authors have suggested that organic species may displace the adsorbed water from the catalyst surface [9,11,14]. Several intermediates can be detected from the IR spectra, such as acetic acid, formaldehyde and formic acid (see Table S1). These intermediates appear to be present in very low concentrations according to the carbon mass balance calculated from acetaldehyde and CO_2 concentrations.

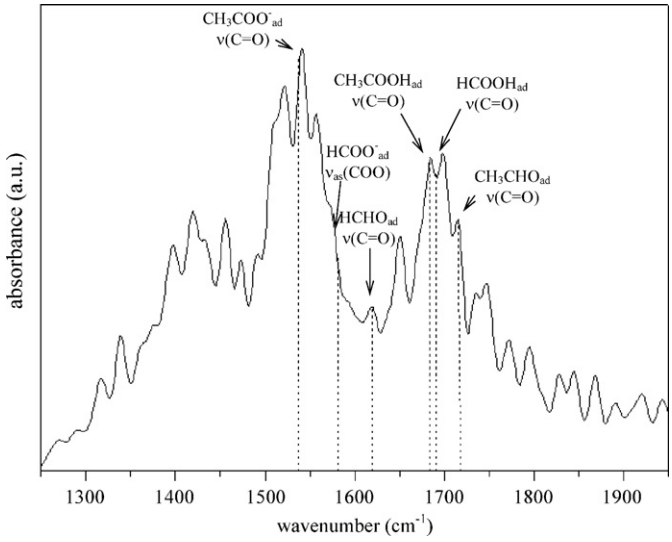

Fig. 5. FTIR spectra of Tsg_NH_3 sample after half of the time necessary for a complete acetaldehyde removal. The curve of the as prepared catalyst was subtracted. The main peaks of adsorbed acetaldehyde and reaction intermediate species, as reported by Yu and Chuang [14], are indicated (see Table S1).

3.4. Photocatalytic experiments under simulated solar and visible irradiation

As underlined in the previous section, the activity sequence of the different samples was the same for the two pollutants; therefore, the role played by a change in the irradiation source was studied only in the case of acetaldehyde.

The reaction rates of acetaldehyde degradation under simulated solar irradiation are reported in Table 1 (6th column), together with the correspondent degradation percentages after 60 min

Table 1
Initial rates of pollutant breakdown for ethanol and acetaldehyde photocatalytic oxidations. The correspondent degradation percentages after a fixed time normalized with respect to the actual surface area of each sample, are also reported.

Sample	Ethanol under UV		Acetaldehyde under UV		Acetaldehyde under SOLAR	
	r_{init}^{EtOH} (mg L^{-1} min^{-1})	% deg (t = 30 min)	r_{init}^{Ac} (mg L^{-1} min^{-1})	% deg (t = 30 min)	r_{init}^{Ac} (mg L^{-1} min^{-1})	% deg (t = 60 min)
Tsg	7.6	32	5.4	12	2.1	10
Tsg_NH_3	8.1	57	5.5	21	2.2	17
Tsg_tea	2.3	14	2.4	8	0.9	6
Tp_NH_3	6.9	51	2.7	11	0.6	5

normalized to the actual surface area of each catalyst (Table 1, 7th column).

The reaction rates of all samples under simulated solar irradiation are much lower than those under UV light. Tsg_NH_3 remains the most active sample. In general, the sequence of sample activity observed under UV irradiation is maintained in simulated solar irradiation. Quite surprisingly, samples with an increased spectral response in the visible did not display an improved activity under solar irradiation. The presence of (a small amount of) UV irradiation in the simulated solar spectra might mask an enhanced activity in the visible of promoted samples. However, Tsg_tea shows a relative photocatalytic improvement under simulated solar irradiation with respect to Tp_NH_3. This fact may be attributable to an increased activity in the visible region.

Tests performed under visible irradiation were not conclusive as the observed decrease in the acetaldehyde peak was comparable with the adsorption phenomena at the catalyst surface and the CO_2 peak remained close to the detection limit of the instrument. The only sample that has shown a detectable visible activity is Tsg_tea, fact that supports our hypothesis of an improved visible activity of this sample. Its activity was nonetheless too faint to give a reliable reaction rate value.

4. Conclusions

N-doped TiO_2 samples are obtained by different synthetic procedures and adopting different N-sources. All samples show a broad absorption in the visible region which is traced back, on the grounds of first principles calculations, to the formation of localized intra-gap electronic levels. Ethanol and acetaldehyde, at concentrations much larger than atmospheric pollution levels, are photodegraded and completely mineralized by all samples. The home-made photocatalysts show the same sequence of activity for the two pollutants indicating that the adsorption/degradation of acetaldehyde is the rate determining step of the process. The most active N-doped sample, both under UV and solar irradiation, is the oxide showing the largest amount of paramagnetic $N_b^{\bullet}$ species.

Under visible irradiation instead, although with very low degree of degradation, the sample which seems to present a larger activity is that one showing the narrowest apparent band gap and the concomitant presence of anatase and brookite polymorphs, which might hinder charge recombination processes.

Acknowledgements

Part of this research was carried out under the Interuniversity attraction poles programme IAP/VI-17 (INANOMAT) financed by the Belgian State, Federal Science Policy Office. The support from the University of Milan research fund (PUR) is also acknowledged.

Appendix A. Supplementary data

Supplementary data associated with this article can be found, in the online version, at doi:10.1016/j.cattod.2010.08.013.

References

[1] R.G. Derwent, M.E. Jenkin, S.M. Saunders, Atmos. Environ. 30 (1996) 181–199.
[2] H.T.-H. Nguyen, N. Takenaka, H. Bandow, Y. Maeda, S.T. de Oliva, M.M.F. Botelho, T.M. Tavares, Atmos. Environ. 35 (2001) 3075–3083.
[3] E.M. Martins, S.M. Correa, G. Arbilla, Atmos. Environ. 37 (2003) 23–29.
[4] M. Colón, J.D. Pleil, T.A. Hartlage, M.L. Guardani, M.H. Martins, Atmos. Environ. 35 (2001) 4017–4403.
[5] S.G. Poulopoulos, H.P. Grigoropoulou, C.J. Philippopoulos, Catal. Lett. 78 (2002) 291–296.
[6] M.L. Sauer, D.F. Ollis, J. Catal. 158 (1996) 570–582.
[7] M.R. Nimlos, E.J. Wolfrum, M.L. Brewer, J.A. Fennell, G. Bintner, Environ. Sci. Technol. 30 (1996) 3102–3110.
[8] D.S. Muggli, J.T. Mccue, J.L. Falconer, J. Catal. 173 (1998) 470–483.
[9] D.S. Muggli, K.H. Lowery, J.L. Falconer, J. Catal. 180 (1998) 111–122.
[10] D.V. Kozlov, E.A. Paukshtis, E.N. Savinov, Appl. Catal. B: Environ. 24 (2000) L7–L12.
[11] E. Piera, J.A. Ayllón, X. Doménech, J. Peral, Catal. Today 76 (2002) 259–270.
[12] J.M. Coronado, S. Kataoka, I. Tejedor-Tejedor, M.A. Anderson, J. Catal. 219 (2003) 219–230.
[13] A.V. Vorontsov, V.P. Dubovitskaya, J. Catal. 221 (2004) 102–109.
[14] Z. Yu, S.S.C. Chuang, J. Catal. 246 (2007) 118–126.
[15] A.V. Emeline, V.N. Kuznetsov, V.K. Rybchuk, N. Serpone, Int. J. Photoenergy (2008) 1–19.
[16] F. Spadavecchia, G. Cappelletti, S. Ardizzone, C.L. Bianchi, S. Cappelli, C. Oliva, P. Scardi, M. Leoni, P. Fermo, Appl. Catal. B: Environ. 96 (2010) 314–322.
[17] C.L. Bianchi, G. Cappelletti, S. Ardizzone, S. Gialanella, A. Naldoni, C. Oliva, C. Pirola, Catal. Today 144 (2009) 31–36.
[18] T. Boiadjieva, G. Cappelletti, S. Ardizzone, S. Rondinini, A. Vertova, Phys. Chem. Chem. Phys. 5 (2003) 1689–1694.
[19] C.A. Paez, D. Poelman, J.-P. Pirard, B. Heinrichs, Appl. Catal. B: Environ. 94 (2010) 263–271.
[20] C. Oliva, L. Bonoldi, S. Cappelli, L. Fabbrini, I. Rossetti, L. Forni, J. Mol. Catal. A: Chem. 226 (2005) 33–40.
[21] G. Kresse, J. Hafner, Phys. Rev. B 47 (1996) 558–561.
[22] G. Kresse, D. Joubert, Phys. Rev. B 59 (1999) 1758–1775.
[23] J.P. Perdew, K. Burke, M. Ernzerhof, Phys. Rev. Lett. 77 (1996) 3865–3868.
[24] K. Eufinger, D. Poelman, H. Poelman, R. De Gryse, G.B. Marin, Appl. Surf. Sci. 254 (2007) 148–152.
[25] D. Meroni, S. Ardizzone, C.L. Bianchi, G. Cappelletti, D. Poelman, H. Poelman, in: XXIII National Congress of the Italian Chemical Society, Sorrento, 5–10 July 2009.
[26] K. Eufinger, PhD thesis, University of Ghent, Belgium, 2007.
[27] M. Bellardita, M. Addamo, A. Di Paola, L. Palmisano, A.M. Venezia, Phys. Chem. Chem. Phys. 11 (2009) 4084–4093.
[28] Di Valentin, E. Finazzi, G. Pacchioni, A. Selloni, S. Livraghi, M.C. Paganini, E. Giamello, Chem. Phys. 339 (2007) 44–56.